Effects of relativity and $M2$ transitions on the resonance contributions to electron-impact ionization of highly charged Li-like ions

M. H. Chen and K. J. Reed

High Temperature Physics Division, Lawrence Livermore National Laboratory, Livermore, California 94550

The effects of relativity on resonance contributions to electron-impact ionization of Ar^{15+}, Fe^{23+}, Kr^{33+}, and Xe^{51+} are investigated. The effects of relativity are found to increase the resonance strengths by 20% for Fe^{23+} and by as much as a factor of 3 for Xe^{51+}. The magnetic quadrupole ($M2$) radiation for the $1s2s2p_{3/2}$ $J=\frac{5}{2}$ metastable state depends strongly on the atomic number, varying as Z^8. We find that including the $M2$ emission for the $1s2s2p_{3/2}$ $J=\frac{5}{2}$ state is essential for obtaining reliable cross sections for ions with $Z \geq 26$.

I. INTRODUCTION

The effects of indirect processes in electron-impact ionization of positive ions have been studied extensively in recent years [1–4]. The most prominent indirect process is excitation of an inner-shell electron followed by emission of an electron and is referred to as excitation-autoionization (EA). The process of resonant capture of the incident electron followed by sequential double autoionization (REDA) has also been shown to contribute significantly to the total-ionization cross section for some ions [2,4].

Earlier theoretical [5–9] and experimental [10–13] studies of electron-impact ionization of ions in the lithiumlike sequence concentrated on low-Z ions. Recently, we calculated cross sections for highly charged Li-like ions with $6 \leq Z \leq 54$ using the relativistic distorted-wave and multiconfiguration Dirac-Fock (MCDF) methods [14,15]. This work included both EA and REDA contributions to the ionization cross sections. We noted that there were prominent REDA resonances which persisted even for high-Z Li-like ions, despite the effects of radiative decay. However, the effects of magnetic quadrupole ($M2$) radiation were omitted in the calculation of the branching ratios for the $1s2s2p_{3/2}$ $^4P_{5/2}$ metastable states, and this could result in an overestimation of the REDA cross sections. In this work we study the effects of the $M2$ emission on the REDA cross sections. We also investigate the effects of relativity on the REDA resonances by computing the resonance strengths using nonrelativistic Hartree-Fock methods, and comparing them with our fully relativistic results.

III. CALCULATIONAL PROCEDURE

For electron-impact ionization of a $2s$ electron of a Li-like ion in the ground state, the direct, excitation-autoionization, and REDA processes can be described schematically by

$$e + 1s^2 2s \rightarrow 1s^2 + e + e , \qquad (1)$$

$$e + 1s^2 2s \rightarrow 1s2snl + e \rightarrow 1s^2 + e + e , \qquad (2)$$

and

$$e + 1s^2 2s \rightarrow 1s2snln'l' \rightarrow 1s2sn''l'' + e \rightarrow 1s^2 + e + e . \qquad (3)$$

Our calculational procedure for these ionization processes has been described in detail in Ref. [14]. Briefly, we performed separate fully relativistic calculations of the direct-ionization cross sections (σ_d), the cross sections for excitation to the intermediate autoionizing states (σ_i^{ex}), the energy-averaged capture cross sections $\bar{\sigma}_k^{cap}$, and the radiative and Auger rates. Assuming that the direct and indirect processes are independent, the total-ionization cross section σ_t is given by

$$\sigma_t = \sigma_d + \sum_i \sigma_i^{ex} B_i^A + \sum_k \bar{\sigma}_k^{cap} B_k^{da} , \qquad (4)$$

where B_i^A and B_k^{da} are the branching ratios for the single and sequential double-Auger emission, respectively.

The relativistic Auger and radiative transition rates [14] were calculated from the perturbation theory using the MCDF method [16,17]. The Auger transition rate in the frozen orbital approximation is given by

$$T = \frac{2\pi}{\hbar} \left| \left\langle \psi_f \left| \sum_{(\alpha < \beta)} V_{\alpha\beta} \right| \psi_i \right\rangle \right|^2 \rho(\varepsilon) , \qquad (5)$$

where ψ_i and ψ_f are the antisymmetrized many-electron wave functions of the initial and final states of the ion, respectively, and $\rho(\varepsilon)$ is the energy density of the final states. The two-electron operator $V_{\alpha\beta}$ in atomic units is taken to be the sum of the Coulomb and generalized Breit operators [18]:

$$V_{12} = \frac{1}{r_{12}} - \boldsymbol{\alpha}_1 \cdot \boldsymbol{\alpha}_2 \frac{\cos(\omega r_{12})}{r_{12}}$$
$$+ (\boldsymbol{\alpha}_1 \cdot \boldsymbol{\nabla}_1)(\boldsymbol{\alpha}_2 \cdot \boldsymbol{\nabla}_2) \frac{\cos(\omega r_{12}) - 1}{\omega^2 r_{12}} . \qquad (6)$$

Here, $\mathbf{r}_1$ and $\mathbf{r}_2$ are particle position vectors with magnitudes r_1 and r_2, respectively, $\mathbf{r}_{12} = \mathbf{r}_1 - \mathbf{r}_2$; and $\boldsymbol{\nabla}_1$ and $\boldsymbol{\nabla}_2$

are gradient operators corresponding to r_1 and r_2, respectively. The α_i are Dirac matrices and ω is the wave number of the exchanged virtual photon.

The spontaneous transition probability for a discrete transition $i \rightarrow f$ in the multipole expansion is given by

$$W_{fi} = \frac{1}{2J_i + 1} \sum_L \frac{2\pi}{2L + 1} |\langle f \| T_L \| i \rangle|^2 . \qquad (7)$$

The reduced matrix element $\langle f \| T_L \| i \rangle$ based on the MCDF model is given in Ref. [16].

The energy levels and bound-state wave functions were calculated explicitly in intermediate coupling with configuration interaction from the same complex using the MCDF model in the average-level scheme [17].

In our previous work the Auger branching ratios for the $1s2s2p_{3/2}$ $J = \frac{5}{2}$ state were set to unity in the calculations of the double-Auger branching ratios B_k^{da}. In this work we have repeated the calculations of the REDA cross sections [the third term of Eq. (4)] with the $M2$ radiation included. We used the atomic data obtained from the previous work [14] for the resonant states $1s2s3lnl'$ ($n = 3$–6, $l \leq 3$) and $1s2s4l4l'$. The nonrelativistic REDA cross sections were also obtained by repeating the calculations with the velocity of light increased a thousandfold to achieve the nonrelativistic limit.

III. RESULTS AND DISCUSSION

In Table I we compare the KMM resonant strengths from several different approximations. In column A we

TABLE I. Resonant energies and strengths for some strong KMM REDA resonances. A: Breit interaction included in Auger transitions but no $M2$ emission included; B: $M2$ emission included but no Breit interaction; C: With Breit interaction and $M2$ emission included. Numbers in brackets are powers of ten.

Autoionizing state	Energy (eV)	Strength (cm²eV)		
		A	B	C
Ar^{15+}				
$1s2s(1)3s^2$ $J = 1$	3230.8	5.19[−21]	5.14[−21]	5.18[−21]
$1s2s(1)3s, \frac{1}{2} 3p_{3/2}$ $J = 2$	3246.7	5.96[−21]	2.78[−21]	5.35[−21]
$1s2s(1)3p_{1/2}, \frac{3}{2} 3p_{3/2}$ $J = 3$	3246.7	5.88[−21]	2.25[−21]	5.17[−21]
$1s2s(1)3p_{1/2}, \frac{1}{2}, 3p_{3/2}$ $J = 2$	3246.8	2.83[−21]	2.03[−21]	2.65[−21]
$1s2s(1)3s, \frac{1}{2} 3d_{3/2}$ $J = 2$	3261.5	2.93[−21]	2.44[−21]	2.82[−21]
$1s2s(1)3s, \frac{1}{2} 3d_{5/2}$ $J = 3$	3261.4	5.35[−21]	3.12[−21]	4.93[−21]
$1s2s(0)3s, \frac{1}{2} 3d_{5/2}$ $J = 2$	3282.0	2.91[−21]	2.89[−21]	2.91[−21]
Fe^{23+}				
$1s2s(1)3s^2$ $J = 1$	6914.5	2.34[−21]	2.33[−21]	2.34[−21]
$1s2s(1)3s, \frac{1}{2} 3p_{3/2}$ $J = 2$	6941.9	3.05[−21]	1.29[−21]	2.17[−21]
$1s2s(1)3p_{1/2}, \frac{3}{2} 3p_{3/2}$ $J = 3$	6942.0	1.89[−21]	5.52[−22]	1.20[−21]
$1s2s(1), 3p_{3/2}^2(2)$ $J = 2$	6965.6	1.36[−21]	1.04[−21]	1.19[−21]
$1s2s(1)3s, \frac{1}{2} 3d_{5/2}$ $J = 3$	6965.7	2.72[−21]	1.41[−21]	2.06[−21]
$1s2s(0)3p_{1/2}, \frac{1}{2} 3p_{3/2}$ $J = 2$	6973.9	1.03[−21]	1.01[−21]	1.03[−21]
$1s2s(1)3p_{3/2}, \frac{5}{2} 3d_{3/2}$ $J = 4$	6981.8	1.23[−21]	2.77[−22]	7.51[−22]
$1s2s(0)3s, \frac{1}{2} 3d_{5/2}$ $J = 2$	6996.0	1.48[−21]	1.46[−21]	1.48[−21]
Kr^{33+}				
$1s2s(1)3s^2$ $J = 1$	13 504.4	9.66[−22]	9.28[−22]	9.58[−22]
$1s2s(1)3s, \frac{3}{2} 3d_{3/2}$ $J = 3$	13 555.4	5.07[−22]	9.31[−23]	1.79[−22]
$1s2s(1)3s, \frac{1}{2} 3p_{3/2}$ $J = 2$	13 556.5	1.51[−21]	5.64[−22]	7.74[−22]
$1s2s(1)3p_{3/2}^2(2)$ $J = 3$	13 595.6	1.30[−21]	4.78[−22]	6.62[−22]
$1s2s(1), 3p_{3/2}^2(2)$ $J = 2$	13 596.7	4.98[−22]	2.60[−22]	3.13[−22]
$1s2s(0)3s, \frac{1}{2} 3p_{3/2}$ $J = 1$	13 601.0	4.27[−22]	4.16[−22]	4.26[−22]
$1s2s(1)3p_{3/2}, \frac{5}{2} 3d_{5/2}$ $J = 4$	13 624.8	5.11[−22]	5.83[−23]	1.54[−22]
$1s2s(0)3p_{3/2}^2(2)$ $J = 2$	13 643.5	6.43[−22]	6.07[−22]	6.25[−22]
Xe^{51+}				
$1s2s(1)3s^2$ $J = 1$	31 389.7	2.44[−22]	1.92[−22]	2.19[−22]
$2s2s(0)3s^2$ $J = 0$	31 475.7	6.69[−23]	5.90[−23]	6.69[−23]
$1s2s(1)3s, \frac{3}{2} 3d_{3/2}$ $J = 3$	31 549.8	6.50[−23]	5.95[−24]	9.32[−24]
$1s2s(1)3s, \frac{1}{2} 3p_{3/2}$ $J = 2$	31 555.4	5.23[−22]	1.47[−22]	1.83[−22]
$1s2s(1)3p_{1/2}, \frac{3}{2} 3p_{3/2}$ $J = 3$	31 567.9	7.63[−23]	2.00[−25]	3.89[−24]
$1s2s(1), 3p_{3/2}^2(2)$ $J = 3$	31 680.6	2.94[−22]	1.23[−23]	2.75[−23]
$1s2s(1)3p_{3/2}, \frac{5}{2} 3d_{5/2}$ $J = 4$	31 755.7	1.01[−22]	2.86[−24]	7.94[−24]
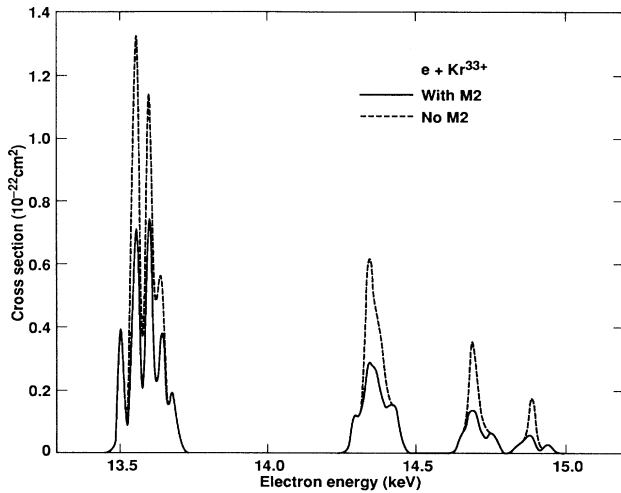
FIG. 1. REDA cross sections for Kr^{33+} as functions of electron energy. The solid curve indicates the results with the Breit interaction and $M2$ emission. The dotted curve displays the values without $M2$ emission.

show the strengths calculated with the Breit interaction included in the Auger transitions, but without the $M2$ contribution. These were taken from Ref. [14]. The results in column B were obtained without the Breit interaction but with the $M2$ contribution included. The results in column C were obtained with both Breit interaction and $M2$ radiation included. The $M2$ emission is important only for the $1s2s2p_{3/2}(J=\frac{5}{2})$ state. The transition from this state is Auger forbidden via Coulomb interaction, as well as electric dipole forbidden. In order to determine accurately the Auger branching for this metastable state, one must include the $M2$ emission and the magnetic and retardation interactions in the Auger calculation. The Breit interaction and other relativistic effects
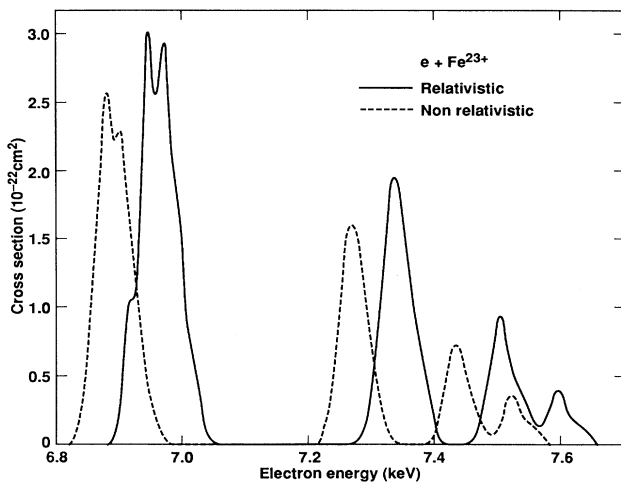
FIG. 2. REDA cross sections for Fe^{23+} as functions of electron energy. The solid curve indicates the results of the relativistic calculation with the Breit interaction and $M2$ emission. The dashed curve displays the results of the nonrelativistic LS-coupling calculation.
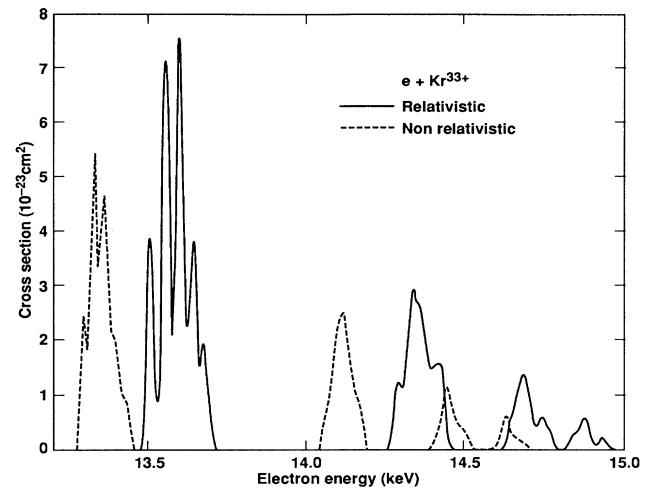
FIG. 3. The REDA cross sections for Kr^{33+}. The symbols are the same as in Fig. 2.

have been found to alter significantly the Auger transition rates for the other $1s2l2l'$ states [19]. Consequently, the branching ratios can be drastically changed by including these relativistic effects.

The resonance strengths for highly charged ions are strongly reduced by the inclusion of the $M2$ emission in cases where the autoionizing states have large branching to the $1s2s2p_{3/2}$ $J=\frac{5}{2}$ state in the first Auger decay [e.g., $1s2s(1)3p_{3/2}$, $\frac{5}{2}$ $3d_{3/2}$ $J=4$]. This is due to the fact that the inclusion of the $M2$ emission results in a large reduction of the Auger branching in the second step. For Ar^{15+}, Fe^{23+}, Kr^{33+}, and Xe^{51+}, the individual KMM resonance strengths are decreased by as much as 15%, 64%, and factors of 3 and 20, respectively. The strong Z dependence can be traced to the fact that the Auger rate from the current-current interaction scales as Z^4, while the $M2$ radiation rises as Z^8 for the $1s2s3p_{3/2}$ $^4P_{5/2}$ state. Hence, the Auger yield of this metastable state falls as Z^{-4} after the inclusion of the $M2$ emission. Neglecting
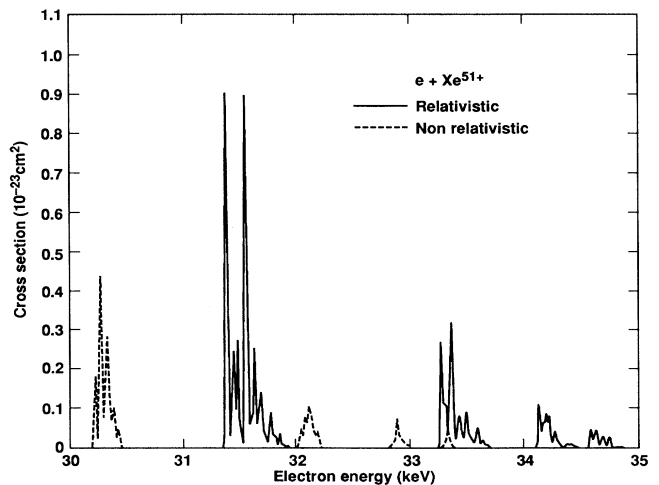
FIG. 4. The REDA cross sections for Xe^{51+}. The symbols are the same as in Fig. 2.
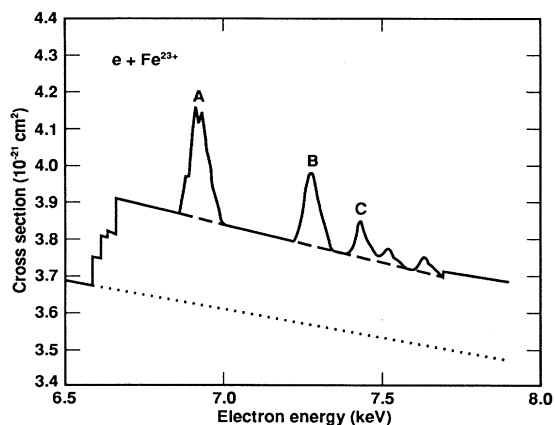
FIG. 5. Electron-impact-ionization cross sections for Fe^{23+} as functions of electron energy. The dotted, dashed, and solid curves show the direct, direct plus EA, and total-ionization cross sections, respectively. The peaks A, B, and C indicate the KMM, KMN, and KMO resonances, respectively.

FIG. 7. Electron-impact-ionization cross sections for Xe^{51+}. The symbols are the same as in Fig. 5.

the Breit interaction in the calculation of the Auger rates, but retaining the $M2$ emission (which is equivalent to setting $B^a = 0$ for the $1s2s2p_{3/2}$ $J = \frac{5}{2}$ state), results in reductions up to factors of 2–10 in the KMM resonance strengths. This clearly demonstrates the importance of the effects of relativity in these cases.

The KMn ($n = 3$–30) resonances for Kr^{33+} are displayed in Fig. 1. The resonances have been convoluted with a 20-eV Gaussian function. It can be seen that the strongest peak is reduced by a factor of 2 when the $M2$ emission is included. The corresponding reduction for Fe^{23+} and Xe^{51+} are factors of 1.5 and 3, respectively.

In Figs. 2–4 the REDA cross sections calculated with relativistic effects and Breit interaction are compared with the nonrelativistic LS-coupling results. The relativistic effects shift the resonances to higher energies by 60, 200, and 1200 eV and enhance the resonance ionization cross sections by 20%, 40%, and a factor of 3 for Fe^{23+}, Kr^{33+}, and Xe^{51+}, respectively. This enhancement is
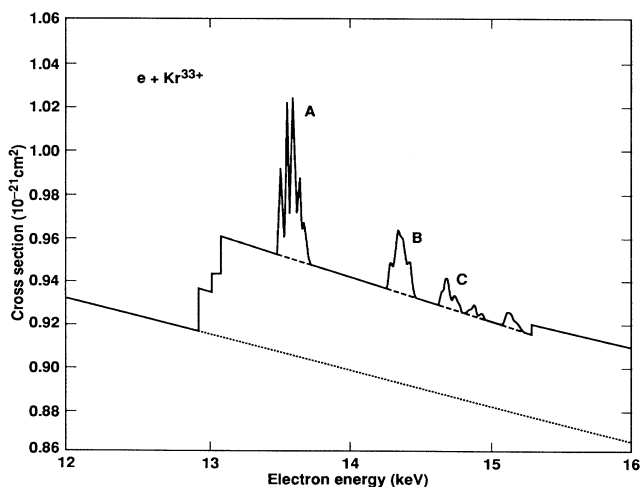
FIG. 6. Electron-impact-ionization cross sections for Kr^{33+}. The symbols are the same as in Fig. 5.
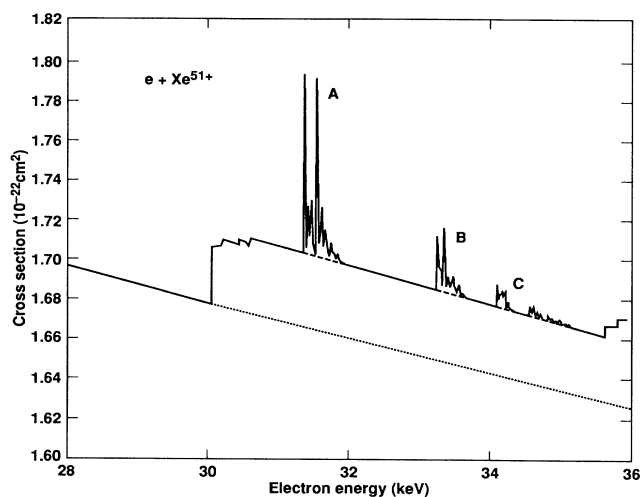
mostly caused by the increase in Auger rates because of the effects of relativity. The effects of relativity on the Auger transition rates can arise from several different factors: (i) changes in energies, (ii) shifts in wave functions, (iii) spin-orbit coupling, and (iv) inclusion of magnetic and retardation interactions in the two-electron operator. For medium-Z ions, the changes in energies and wave functions modify the KLL Auger rates by as much as a factor of 2, while the effect of current-current interaction increases the rates by nearly a factor of 4 in some cases [19]. For high-spin metastable states (e.g., $1s2s2p\ ^4P$), the spin-orbit coupling and magnetic interaction are the dominant factors in the Auger decay [19].

In Figs. 5–7 we show the total-ionization cross sections obtained by adding the direct and excitation-autoionization cross sections from our previous work [14] to the new REDA cross sections. The peaks labeled A, B, and C are the KMM, KMN, and KMO resonances, respectively. Near the region of the KMM resonances, the indirect processes contribute about 15%, 11%, and 8% for Fe^{23+}, Kr^{33+}, and Xe^{51+}. This gradual decrease in the importance of the indirect contribution is due to the increasing dominance of radiative decay with increasing atomic number. The total-ionization cross sections are within 20% of the results obtained by Badnell and Pind-zola [20] using semirelativistic wave functions.

In summary, we have studied the effects of relativity and $M2$ emission on the resonance contributions to the electron-impact-ionization cross sections for highly charged Li-like ions. We note that it is essential to include the effects of relativity and intermediate coupling as well as the $M2$ emission for the $1s2s2p_{3/2}$ $J = \frac{5}{2}$ state to obtain reliable cross sections.

ACKNOWLEDGMENTS

[1] R. A. Falk *et al.*, Phys. Rev. Lett. **47**, 494 (1981).

[2] K. T. LaGattuta and Y. Hahn, Phys. Rev. A **24**, 2273 (1981).

[3] D. C. Griffin *et al.*, Phys. Rev. A **29**, 1729 (1984).

[4] M. H. Chen, K. J. Reed, and D. L. Moores, Phys. Rev. Lett. **64**, 1350 (1990).

[5] S. S. Tayal and R. J. W. Henry, Phys. Rev. A **42**, 1831 (1990).

[6] R. J. W. Henry, J. Phys. B **12**, L309 (1979).

[7] S. S. Tayal and R. J. W. Henry, Phys. Rev. A **44**, 2955 (1991).

[8] H. Jakubowiz and D. L. Moores, J. Phys. B **14**, 3733 (1981).

[9] M. S. Pindzola and D. C. Griffin, Phys. Rev. A **36**, 2628 (1987).

[10] A. Müller, G. Hofmann, K. Tinschert, and E. Salzborn, Phys. Rev. Lett. **61**, 1352 (1988).

[11] G. Hofmann, A. Müller, K. Tinschert, and E. Salzborn, Z. Phys. D **16**, 113 (1990).

[12] D. H. Crandall, R. A. Phaneuf, D. C. Gregory, A. M. Howald, D. W. Müller, T. J. Morgan, G. H. Dunn, D. C. Griffin, and R. J. W. Henry, Phys. Rev. A **34**, 1757 (1986).

[13] D. H. Crandall, R. A. Phaneuf, B. E. Hasselquist, and D. C. Gregory, J. Phys. B **12**, L249 (1979).

[14] M. H. Chen and K. J. Reed, Phys. Rev. A **45**, 4525 (1992).

[15] K. J. Reed and M. H. Chen, Phys. Rev. A **45**, 4519 (1992).

[16] M. H. Chen, Phys. Rev. A **31**, 1449 (1985).

[17] I. P. Grant *et al.*, Comput. Phys. Commun. **21**, 207 (1980).

[18] J. B. Mann and W. R. Johnson, Phys. Rev. A **4**, 41 (1971).

[19] M. H. Chen, *Proceedings of the Fifteenth International Conference on X-Ray and Inner-Shell Processes,* edited by T. A. Carlson, M. O. Krause, and S. T. Manson, AIP Conf. Proc. No. 215 (AIP, New York, 1990), p. 391; Nucl. Instrum. Methods B **43**, 366 (1989).

[20] N. R. Badnell and M. S. Pindzola, Phys. Rev. A **47**, 2937 (1993).